

A COMPARATIVE STUDY ON MHD FORCED CONVECTIVE FLOW OF DIFFERENT NANOFUIDS WITH WATER (H₂O) AS BASE FLUID IN A VERTICAL RECTANGULAR DUCT

 **Bishnu Ram Das***,  **P.N. Deka#**

Department of Mathematics, Dibrugarh University, Dibrugarh-786004, Assam, India

**Corresponding Author e-mail: e-mail: bishnuram.das84@gmail.com; #pndeka@dibru.ac.in*

Received December 21, 2023; revised January 24, 2024; accepted January 28, 2024

In this paper, a comparative study on MHD forced convective flow for heat transfer efficiency of different nanofluids with water (H₂O) as base fluid has been carried out. Here, in this study flow through vertical rectangular has been considered in presence of strong magnetic field. In this laminar flow we consider duct walls as electrically non-conducting where the transverse magnetic field acting normally on the duct walls. Joule heat and the viscous dissipation effects are included in the energy equation and furthermore the walls of the duct are kept at constant temperature. An explicit finite difference method has been adopted with fine grid in the control volume for solving the governing equations of this MHD nanofluid flow. Computational processes are carried out using MATLAB code. In this present work we have plotted the flow fields velocity, induced magnetic field, and temperature for various values of MHD flow parameters graphically by varying thermal Grashof number (G_r), Hartmann number (Ha), Reynold number (R_e), Eckert number (Ec), Prandtl number (P_r), magnetic Reynold number (R_m), and nanoparticle volume fraction (ϕ) respectively.

Keywords: *MHD forced convective flow; Nanofluids; Steady; Explicit finite difference method (EFDM); Vertical rectangular duct*

PACS: 95.30.Qd, 94.30.cq, 94.30.Kq

1. INTRODUCTION

Inclusion of nanoparticles in the base fluid is an innovative way to enhance heat transfer. There are large variety of nanoparticles used in water based nanofluids and each of them exhibit performance in heat transfer process and possess different nanofluid flow characteristics. Nanofluids have better suspension stability, Newtonian behavior, healthier thermal conductivity, and huge chaotic movements of nanoparticles are believed to be liable for the increased of heat transfer characteristic. In natural convection, the base fluid has a low thermal conductivity, which limits the heat transfer performance. Use of nanofluid is an innovative technique in which the colloidal suspension of nanometer sized particles in a base fluid (nanofluid) was first introduced by Choi [1] at the Argonne National Laboratory, U.S.A.

Latter, Lee *et al.* [2] analyze the thermal conductivity of nonidentical metal oxides and in this way, they have got the shape and size provide considerably to the more acceptable thermal conductivity of the nanofluid. Forced convection is the most important aspect investigation for applications in a rectangular duct. The applications are thermal power plants, solar collectors, chemical catalytic reactors and cooling systems. Thermal conductivity of TiO₂/water nano-fluid up to 7.5% nanoparticle concentration experimentally found by Xuan *et al.* [3]. Heat transfer efficiency with nano-fluid was examined by many researchers [4, 5].

In another study Ellahi *et al.* [6] considered water base nanofluid with Al₂O₃ as nanoparticles to study aggregation effect on such nanofluid having permeable wedge in the presence of mixed convection. An analytical solution of natural convection flow problem nanofluid over a linearly stretching sheet under magnetic field was attempted by Hamad [7]. Kodi *et al.* [8] investigated influence of MHD mixed convection flow for Maxwell nanofluid through a vertical cone with porous material in the existence of variable heat conductivity and diffusion. Ragulkumar *et al.* [9] studied dissipative MHD free convective nanofluid flow past a vertical cone under radiative chemical reaction with mass flux.

Mixed convection of Casson nanofluid over a stretching sheet with convectively heated chemical reaction and heat source/sink observed by Hayat *et al.* [10]. The focus of this study is to learn about the effects of solid volume fraction on heat transfer quantity and on differential pressure. It was about in the such that increasing concentration of nanoparticle has no significant effect on heat transfer but pressure drop enhancement has affected on heat transfer process. Ferdows *et al.* [11] considered nanofluid inclusion with diverse types of nanoparticles for the incompressible, laminar, steady and convective viscous flow. They observed that heat transfer was constantly increased with increase value of nanoparticle volume fraction parameter. Numerical investigation of solar radiation on the effects on heat-mass transfer phenomena of nanofluids recently studied by [12, 13] Rao and Deka. In another study, very recently Das *et al.* [14] investigated in a vertical square duct numerical analysis on magnetohydrodynamics (MHD) mixed convection flow of Al₂O₃/water nanofluids. Many authors who had investigated heat transfer nanofluids boundary layer problem given in ref. [15, 16]. Paul *et al.* [17] studied Darcy-Forchheimer MHD radiative flow through a porous space incorporating viscous dissipation, heat source, and chemical reaction effect across an exponentially stretched surface. Arruna *et al.* [18] have been investigated effect of chemical reaction and radiation absorption on MHD Casson fluid over an exponentially stretching sheet with slip conditions: ethanol as solvent. On a non-Newtonian nanofluid flow and heat mass transfer in a two-dimensional steady laminar boundary layer caused by a horizontally stretching sheet investigated by

Alrihieli *et al.* [19]. The study includes heat generation/absorption near a stagnation point and on the radially stretching plate. In a vertical stretching surface Jawad [20] studied on magnetohydrodynamics (MHD) stagnation point flow of micropolar fluids with buoyancy and thermal radiation. Shoeibi *et al.* [21] have been observed about the utilize of hybrid nanofluids in solar system. In a vertical duct containing metallic/carbon nanofluids Beg *et al.* [22] have been studied with Dufour and Soret double cross repetition counting of thermo-solutal convection. Bhatti *et al.* [23] have been studied swimming of Gyrotactic microorganism in MHD Williamson nanofluid flow between rotating circular plates embedded in porous medium. Hussain *et al.* [24] have been investigated MHD instability of Hartmann flow of nanoparticles Fe_2O_3 in water. [25] Umavathi and Beg investigated double diffusive convection in a dissipative electrically conducting nanofluid under orthogonal electrical and magnetic fields. [26] Bhatti and Abdelsalam observed Bio-inspired peristaltic propulsion of hybrid nanofluid flow with Tantalum (Ta) and Gold (Au) nanoparticles under magnetic effects.

The aim of this present work is to numerically investigate the laminar steady forced convective flow of different nanofluids with water (H_2O) as base fluid in presence of strong magnetic field in a vertical rectangular duct. We have presented result of our investigation for different type of nanofluid flow and we have drawn conclusion heat transfer efficiency of different water based nanofluid.

Table (i). Numerical values of water (H_2O) and nanoparticles titanium oxide (TiO_2), aluminium oxide (Al_2O_3), ferric oxide (Fe_2O_3), and silicon oxide (SiO_2)

	Density (ρ)	Specific heat capacity (C_p)	Thermal conductivity (k)	Electrical conductivity (σ)
H_2O	997.1	4179	0.613	5.5×10^{-6}
TiO_2	4250	686.2	8.9528	2.58×10^{-7}
Al_2O_3	3970	765	40	35×10^6
Fe_2O_3	5180	765	9.7	25×10^3
SiO_2	2200	703	1.2	2.58×10^{-7}

2. MATHEMATICAL FORMULATION

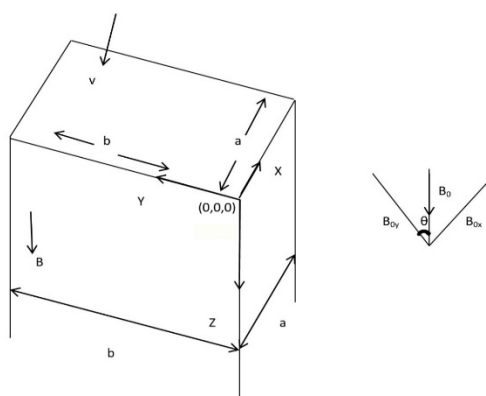


Figure 1. Physical configuration

In this paper, we have considered a laminar steady flow of incompressible fluid through a duct which is vertically positioned, where cross section of the duct has length a and breadth b . Both the parallel walls of the duct are kept at $x = 0$ and $x = a$, and the other parallel walls are kept at $y = 0$ and at $y = b$. Here we consider that the duct has cross section on the xy - plane where the fluid velocity, induced magnetic field and temperature are in the z -direction. In this case applied uniform magnetic field B_o of the fluid acts in a direction lying in the xy - plane but making an angle θ with the y -axis. The flow is handled in presence of a constant pressure gradient $\frac{\partial p}{\partial z}$ and the MHD force. In this work, the physical parameters except pressure are independent of variable z , the fluid properties in the buoyancy term are considered as constant. Moreover, Joule heating and the effects of viscous dissipation are considered in the energy equation. Our fluid is viscous and incompressible and flow is laminar and steady. We have also assumed that there is no net flow of current in the z -direction. The velocity, induced magnetic field, and the temperature \vec{V} , \vec{B} , and T as:

$$\vec{V} = \{0, 0, V_z(x, y)\}, \vec{B} = \{B_{ox}, B_{oy}, B_z(x, y)\}, T = T(x, y) \text{ in where } B_{ox} = B_o \sin \theta, B_{oy} = B_o \cos \theta$$

3. GOVERNING EQUATIONS

Equation of continuity is

$$\nabla \cdot \vec{V} = 0. \quad (1)$$

The MHD momentum equation is

$$\rho_{nf} \left[\frac{\partial \vec{V}}{\partial t} + (\vec{V} \cdot \nabla) \vec{V} \right] = -\nabla p + \mu_{nf} \nabla^2 \vec{V} + (\vec{J} \times \vec{B}) + \vec{X}, \quad (2)$$

in where $\vec{X} = g(\rho\beta)_{nf}(T - T_o)$
 Maxwell's equation is

$$\nabla \cdot \vec{B} = 0. \tag{3}$$

Ampere's law

$$\nabla \times \vec{B} = (\mu_e)_{nf}\vec{J}. \tag{4}$$

Definition of Ohm's law:

$$\vec{J} = \sigma_{nf}(\vec{E} + \vec{V} \times \vec{B}). \tag{5}$$

Equation of magnetic induction is

$$\frac{\partial \vec{B}}{\partial t} = \nabla \times (\vec{V} \times \vec{B}) + \lambda_{nf}\nabla^2 \vec{B}. \tag{6}$$

Now using equation (1) & equation (3) in equation (6) we get

$$\frac{\partial \vec{B}}{\partial t} + (\vec{V} \cdot \nabla)\vec{B} = (\vec{B} \cdot \nabla)\vec{V} + \lambda_{nf}\nabla^2 \vec{B}. \tag{7}$$

The Energy equation is

$$(\rho C_p)_{nf} \left[\frac{\partial T}{\partial t} + (\vec{V} \cdot \nabla)T \right] = k_{nf}\nabla^2 T + \mu_{nf}\phi + \frac{J^2}{\sigma_{nf}}. \tag{8}$$

Again, we get

$$\nu_{nf} = \frac{\mu_{nf}}{\rho_{nf}}. \tag{9}$$

and

$$\lambda_{nf} = \frac{1}{\sigma_{nf}(\mu_e)_{nf}} \tag{10}$$

We know that the dynamic viscosity of nanofluid, effective density of nanofluid, magnetic permeability of nanofluid, electrical conductivity of nanofluid, heat capacity of nanofluid, thermal expansion coefficient of nanofluid, and thermal conductivity of nanofluid as:

$$\mu_{nf} = \mu_f(1 - \phi)^{-2.5}, \tag{11}$$

$$\rho_{nf} = \left[1 - \phi + \phi \frac{\rho_s}{\rho_f} \right] \rho_f, \tag{12}$$

$$(\mu_e)_{nf} = \left[1 - \phi + \phi \frac{(\mu_e)_s}{(\mu_e)_f} \right] (\mu_e)_f, \tag{13}$$

$$\sigma_{nf} = \left[1 + \frac{3(\sigma-1)\phi}{(\sigma+2)-(\sigma-1)\phi} \right] \sigma_f, \tag{14}$$

$$(\rho C_p)_{nf} = \left[1 - \phi + \phi \frac{(\rho C_p)_s}{(\rho C_p)_f} \right]. \tag{15}$$

$$(\rho\beta)_{nf} = \left[1 - \phi + \phi \frac{(\rho\beta)_s}{(\rho\beta)_f} \right] (\rho\beta)_f \tag{16}$$

$$k_{nf} = \left[\frac{k_s+2k_f-2\phi(k_f-k_s)}{k_s+2k_f+\phi(k_f-k_s)} \right] k_f. \tag{17}$$

For the problem the corresponding the initial & boundary conditions are given by

$$\begin{aligned} V_z = 0, B_z = 0, T = T_o, \text{ when } x = 0 \\ V_z = 0, B_z = 0, T = T_o, \text{ when } x = a, \text{ for } 0 \leq y \leq b \\ V_z = 0, B_z = 0, T = T_o, \text{ when } y = 0 \\ V_z = 0, B_z = 0, T = T_o, \text{ when } y = b, \text{ for } 0 \leq x \leq b. \end{aligned} \tag{18}$$

The following dimensionless variables:

$$\bar{V} = \frac{V}{V_o}, \bar{B} = \frac{B}{B_o}, \bar{T} = \frac{T-T_o}{\Delta T}, \bar{x} = \frac{x}{a}, \bar{y} = \frac{y}{Aa}, \tag{19}$$

where:

$$A = \frac{b}{a}, B_o = -a^2(\mu_e)_{nf} \sqrt{\frac{\sigma_{nf}}{\rho_{nf}\nu_{nf}}} \frac{\partial p}{\partial z}, V_o = -\frac{a^2}{\rho_{nf}\nu_{nf}} \frac{\partial p}{\partial z}, T - T_o = \frac{V_o^2}{(C_p)_f},$$

Now using above dimensionless parameters and after simplification we get,

$$\frac{\partial^2 V}{\partial x^2} + \frac{1}{A^2} \frac{\partial^2 V}{\partial y^2} + \frac{B_0^2 a^2 \left[1 + \frac{3(\sigma-1)\phi}{(\sigma+2)-(\sigma-1)\phi} \right] \frac{\sigma_f}{\mu_f} (1-\phi)^{2.5}}{V_0 a \left[1 - \phi + \phi \frac{(\mu_e)_s}{(\mu_e)_f} \right] (\mu_e)_f \left[1 + \frac{3(\sigma-1)\phi}{(\sigma+2)-(\sigma-1)\phi} \right] \sigma_f} \sin\theta \frac{\partial B}{\partial x} + \frac{1}{A} \frac{B_0^2 a^2 \left[1 + \frac{3(\sigma-1)\phi}{(\sigma+2)-(\sigma-1)\phi} \right] \frac{\sigma_f}{\mu_f} (1-\phi)^{2.5}}{V_0 a \left[1 - \phi + \phi \frac{(\mu_e)_s}{(\mu_e)_f} \right] (\mu_e)_f \left[1 + \frac{3(\sigma-1)\phi}{(\sigma+2)-(\sigma-1)\phi} \right] \sigma_f} \cos\theta \frac{\partial B}{\partial y} + \frac{g\beta_f a^3 (T-T_0)}{\nu_f^2} \cdot \frac{\nu_f}{V_0 a} T + 1 = 0. \quad (20)$$

$$\frac{\partial^2 B}{\partial x^2} + \frac{1}{A^2} \frac{\partial^2 B}{\partial y^2} + V_0 a \left[1 - \phi + \phi \frac{(\mu_e)_s}{(\mu_e)_f} \right] (\mu_e)_f \left[1 + \frac{3(\sigma-1)\phi}{(\sigma+2)-(\sigma-1)\phi} \right] \sigma_f \sin\theta \frac{\partial V}{\partial x} + \frac{1}{A} V_0 a \left[1 - \phi + \phi \frac{(\mu_e)_s}{(\mu_e)_f} \right] (\mu_e)_f \left[1 + \frac{3(\sigma-1)\phi}{(\sigma+2)-(\sigma-1)\phi} \right] \sigma_f \cos\theta \frac{\partial V}{\partial y} = 0. \quad (21)$$

$$\frac{\partial^2 T}{\partial x^2} + \frac{1}{A^2} \frac{\partial^2 T}{\partial y^2} + \frac{\mu_f C_p}{(1-\phi)^{2.5} k_f \left[\frac{k_s + 2k_f - 2\phi(k_f - k_s)}{k_s + 2k_f + \phi(k_f - k_s)} \right]} \cdot \frac{V_0^2}{C_p \Delta T} \left[\left(\frac{\partial V}{\partial x} \right)^2 + \frac{1}{A^2} \left(\frac{\partial V}{\partial y} \right)^2 \right] + \frac{B_0^2 a^2 \left[1 + \frac{3(\sigma-1)\phi}{(\sigma+2)-(\sigma-1)\phi} \right] \frac{\sigma_f}{\mu_f}}{V_0^2 a^2 \left[1 - \phi + \phi \frac{(\mu_e)_s}{(\mu_e)_f} \right]^2 \left[1 + \frac{3(\sigma-1)\phi}{(\sigma+2)-(\sigma-1)\phi} \right]^2 \sigma_f^2 (\mu_e)_f^2 \left[\frac{k_s + 2k_f - 2\phi(k_f - k_s)}{k_s + 2k_f + \phi(k_f - k_s)} \right]} \cdot \frac{\mu_f C_p}{k_f} \cdot \frac{V_0^2}{C_p \Delta T} \left[\left(\frac{\partial B}{\partial x} \right)^2 + \frac{1}{A^2} \left(\frac{\partial B}{\partial y} \right)^2 \right] = 0. \quad (22)$$

Let

$$E_1 = \frac{1}{(1-\phi)^{2.5}}, E_2 = \left[1 - \phi + \phi \frac{\rho_s}{\rho_f} \right], E_3 = \left[1 - \phi + \phi \frac{(\mu_e)_s}{(\mu_e)_f} \right], E_4 = \left[1 + \frac{3(\sigma-1)\phi}{(\sigma+2)-(\sigma-1)\phi} \right], E_5 = \left[1 - \phi + \phi \frac{(\rho C_p)_s}{(\rho C_p)_f} \right], E_6 = \left[1 - \phi + \phi \frac{(\rho\beta)_s}{(\rho\beta)_f} \right], E_7 = \left[\frac{k_s + 2k_f - 2\phi(k_f - k_s)}{k_s + 2k_f + \phi(k_f - k_s)} \right]$$

Therefore, the equations (20), (21), (22) in terms $E_1, E_2, E_3, E_4, E_5, E_6, E_7$ are

$$\frac{\partial^2 V}{\partial x^2} + \frac{1}{A^2} \frac{\partial^2 V}{\partial y^2} + \frac{Ha^2}{R_m} \sin\theta \frac{E_4}{E_1 E_3 E_4} \frac{\partial B}{\partial x} + \frac{1}{A} \frac{Ha^2}{R_m} \cos\theta \frac{E_4}{E_1 E_3 E_4} \frac{\partial B}{\partial y} + \frac{G_r}{R_e} T + 1 = 0. \quad (23)$$

$$\frac{\partial^2 B}{\partial x^2} + \frac{1}{A^2} \frac{\partial^2 B}{\partial y^2} + R_m \sin\theta E_3 E_4 \frac{\partial V}{\partial x} + \frac{1}{A} R_m \cos\theta E_3 E_4 \frac{\partial V}{\partial y} = 0. \quad (24)$$

$$\frac{\partial^2 T}{\partial x^2} + \frac{1}{A^2} \frac{\partial^2 T}{\partial y^2} + \frac{E_1}{E_7} P_r Ec \left[\left(\frac{\partial V}{\partial x} \right)^2 + \frac{1}{A^2} \left(\frac{\partial V}{\partial y} \right)^2 \right] + \frac{Ha^2 P_r Ec}{R_m^2} \frac{E_4}{E_3^2 E_4^2 E_7} \left[\left(\frac{\partial B}{\partial x} \right)^2 + \frac{1}{A^2} \left(\frac{\partial B}{\partial y} \right)^2 \right] = 0. \quad (25)$$

Where:

$Ha = B_0 a \sqrt{\frac{\sigma_f}{\mu_f}}$, is the Hartmann number,

$G_r = \frac{g\rho_f\beta_f(T-T_0)a^3}{\mu_f^2}$, is the thermal Grashof number,

$P_r = \frac{\mu_f(Cp)_f}{k_f}$, is the Prandtl number,

$Ec = \frac{V_0^2}{(Cp)_f \Delta T}$, is the Eckert number,

$R_e = \frac{V_0 a}{\mu_f}$, is the Reynolds number,

and

$R_m = V_0 a (\mu_e)_f \sigma_f$, is the magnetic Reynolds number

The corresponding boundary conditions (21) gives

$$\begin{aligned} V = 0, B = 0, T = 0, \text{ when } x = 0 \\ V = 0, B = 0, T = 0, \text{ when } x = 1, \text{ for } 0 \leq y \leq A \\ V = 0, B = 0, T = 0, \text{ when } y = 0 \\ V = 0, B = 0, T = 0, \text{ when } y = A, \text{ for } 0 \leq x \leq 1. \end{aligned} \quad (26)$$

4. NUMERICAL TECHNIQUE AND GRID INDEPENDENCE STUDY

With the boundary conditions given in equation (26), the dimensionless governing equations (23), equation (24) and equation (25) were discretized using explicit finite difference method. We know that the finite difference second order $\frac{\partial^2 V}{\partial x^2}$ and the first order $\frac{\partial V}{\partial x}$, were discretized as $\frac{\partial^2 V}{\partial x^2} = \frac{V_{i+1,j} - 2V_{i,j} + V_{i-1,j}}{\Delta x^2} + O(\Delta x^2)$ and $\frac{\partial V}{\partial x} = \frac{V_{i+1,j} - V_{i-1,j}}{2\Delta x} + O(\Delta x^2)$, respectively. Therefore, after simplification the equations (23), (24), and (25) we get

$$V_{i,j} = A_9(V_{i+1,j} + V_{i-1,j}) + A_{10}(V_{i,j+1} + V_{i,j-1}) + A_{11}(B_{i+1,j} - B_{i-1,j}) + A_{12}(B_{i,j+1} - B_{i,j-1}) + A_{13}(T_{i,j}) + A_{14}, \tag{27}$$

$$B_{i,j} = A_9(B_{i+1,j} + B_{i-1,j}) + A_{10}(B_{i,j+1} + B_{i,j-1}) + A_{15}(V_{i+1,j} - V_{i-1,j}) + A_{16}(V_{i,j+1} - V_{i,j-1}), \tag{28}$$

$$T_{i,j} = A_9(T_{i+1,j} + T_{i-1,j}) + A_{10}(T_{i,j+1} + T_{i,j-1}) + A_{17}(V_{i+1,j} - V_{i-1,j})^2 + A_{18}(V_{i,j+1} - V_{i,j-1})^2 + A_{19}(B_{i+1,j} - B_{i-1,j})^2 + A_{20}(B_{i,j+1} - B_{i,j-1})^2, \tag{29}$$

Where $A_1 = \frac{1}{A^2}$, $A_2 = \frac{(Ha)^2}{(R_m)} \sin\theta \frac{E_4}{E_1 E_3 E_4} \theta$, $A_3 = \frac{1}{A} \frac{(Ha)^2}{(R_m)} \cos\theta \frac{E_4}{E_1 E_3 E_4}$, $A_4 = \frac{(G_r)}{(R_e)}$, $A_5 = \frac{k^2}{2(A_1 h^2 + k^2)}$, $A_6 = \frac{A_1 h^2}{2(A_1 h^2 + k^2)}$, $A_7 = \frac{A_2 h k^2}{2(A_1 h^2 + k^2)}$, $A_8 = \frac{A_3 h^2 k}{2(A_1 h^2 + k^2)}$, $A_9 = \frac{A_4 h^2 k^2}{A_1 h^2 + k^2}$, $A_{10} = \frac{h^2 k^2}{A_1 h^2 + k^2}$, $A_{11} = R_m \sin\theta E_3 E_4$,

$A_{12} = \frac{1}{A} R_m \cos\theta E_3 E_4$, $A_{13} = \frac{A_{11} h k^2}{2(A_1 h^2 + k^2)}$, $A_{14} = \frac{A_{12} h^2 k}{2(A_1 h^2 + k^2)}$, $A_{15} = \frac{E_1}{E_6} P_r E_c$, $A_{16} = \frac{(Ha)^2 (E_c) (P_r)}{(R_m)^2} \frac{E_4}{E_3^2 E_4^2 E_6}$, $A_{17} = \frac{A_{15} k^2}{4(A_1 h^2 + k^2)}$, $A_{18} = \frac{A_1 A_{15} h^2}{4(A_1 h^2 + k^2)}$, $A_{19} = \frac{A_{16} k^2}{4(A_1 h^2 + k^2)}$, $A_{20} = \frac{A_1 A_{16} h^2}{4(A_1 h^2 + k^2)}$,

are constants and in where $\Delta x = h = 0.001$ and $\Delta y = k = 0.001$.

Discretized boundary conditions are given by

$$\begin{aligned} V_{i,1} &= 0, B_{i,1} = 0, T_{i,1} = 0, \text{ when } j = 1 \\ V_{i,m+1} &= 0, B_{i,m+1} = 0, T_{i,m+1} = 0, \text{ when } j = n + 1, \\ &\text{for } 1 \leq i \leq m + 1 \\ V_{1,j} &= 0, B_{1,j} = 0, T_{1,j} = 0, \text{ when } i = 1 \\ V_{m+1,j} &= 0, B_{m+1,j} = 0, T_{m+1,j} = 0, \text{ when } i = m + 1 \\ &\text{for } 1 \leq j \leq n + 1, \end{aligned} \tag{30}$$

5. RESULTS AND DISCUSSION

The outcome of parameters like, thermal Grashof number (G_r), Hartmann number (Ha), Reynold number (R_e), Prandtl number (P_r), Eckert number (Ec), magnetic Reynold number (R_m), and the nanoparticle volume fraction (ϕ) on the velocity, induced magnetic field, and temperature distributions are exhibits in graphical presentation. We have taken $Ha = 2$, $A = 2.5$, $P_r = 6.93$, $R_m = 1$, $Ec = 0.001$, $h = k = 0.001$, $m = n = 200$, $\phi = 0.02$, $k_f = 0.613$, $k_s = 429$, $\theta = \pi/2$.

The graphs are plotted by utilizing numerical out come through an explicit finite difference method in MATLAB operating system. The velocity distribution of titanium oxide/water nanofluid for various values of Hartmann number (Ha) is depicted in **Figure 2**. We have observed from **Figure 2** that the fluid velocity distribution decreases due to increase in value of Hartmann number (Ha). We know that in the middle of the rectangular duct, the fluid has maximum value of velocity, so in this step the electromagnetic force resists the fluid's motion and this electromagnetic force slow down convection a flatten velocity distribution. Similar nature of induced magnetic field is observed and seen in **Figure 3**. Further, in **Figure 4**. It is observed that temperature (T) is increased with increased value of Hartmann number (Ha) in boundary layer region. The magnetic field introduced to the electrically conducting nanofluid and acting normal to boundary is responsibility for resistive pressure force in the duct which is part of Lorentz force. In the cooling sector magnetic field's effect on nanofluid has many industrial accomplishments too. The velocity distribution of titanium oxide/water nanofluid for various values of thermal Grashof number (G_r) is depicted in Fig. 5. We have seen in **Figure 5** that the velocity distribution enhanced owing to enhancement of parametric values of the thermal Grashof number (G_r). An enlarge in the value of thermal Grashof number has the tendency to induce much flow in the boundary layer due to the effect of thermal buoyancy. Similar nature we have observed in induced magnetic field in **Figure 6**. But it is observed in **Figure 7**, that the temperature profile decreases owing to increase in parametric value of thermal Grashof number (G_r). This means that buoyancy force decreases the temperature field. The velocity distribution of titanium oxide/water nanofluid for different values of Reynold number (R_e) is depicted in **Figure 8**.

It is observed from **Figure 8**, that the velocity profile enhanced owing to enhancement of parametric values of Reynold number (Re). Due to enhancement in values of (Re), in the thermal boundary layer, frictional heating increases.

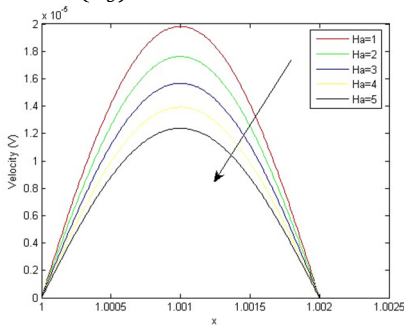


Figure 2. Variation in (V) with Ha

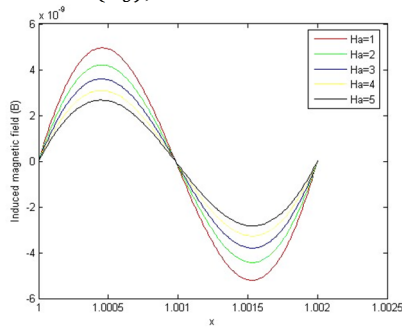


Figure 3. Variation in (B) with Ha

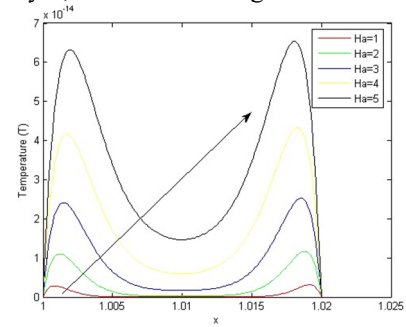


Figure 4. Variation in (T) with Ha

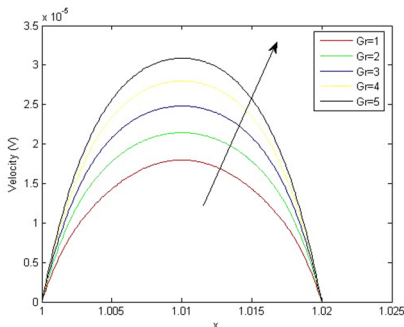


Figure 5. Variation in (V) with Gr

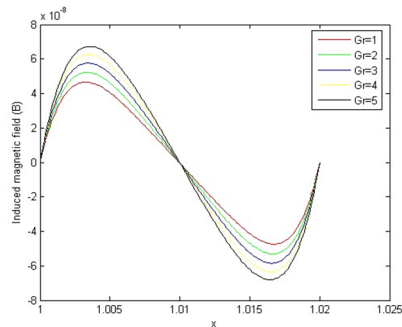


Figure 6. Variation in (B) with Gr

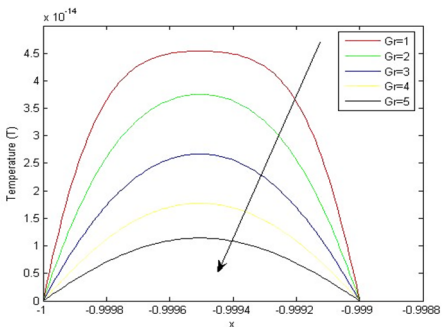


Figure 7. Variation in (T) with Gr

This in results reflect in enhancement of kinetic energy of the fluid particles in the middle layers as a consequence we have the flow rate accelerates and, in this way, increases the velocity. Similar effect we have observed in induced magnetic field in **Figure 9**. The temperature distribution of titanium oxide/water nanofluid for different values of Reynold number (Re) is depicted in **Figure 10**. But we have seen in **Figure 10**, that the temperature profile decreases due to increase in value of Reynold number (Re). The increase in values of Reynold number (Re) enhanced the strength of the discharge velocity on the plate which minimizes the growth of thermal boundary layer. This diminishes the temperature near to the plate surface. The velocity distribution of titanium oxide/water nanofluid for distinct values of Prandtl number (Pr) is represented in graph given in **Figure 11**. We have seen in **Figure 11**, that the velocity profile is enhanced owing to enhancement in the value of Prandtl number (Pr). Due to impact of additional nanoparticles periodic motion of nanoparticle is observed an increase of Prandtl number (Pr). So, the kinetic energy is transform into heat energy, and so the velocity increases.

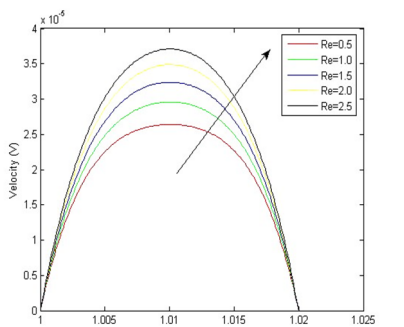


Figure 8. Variation in (V) with Re

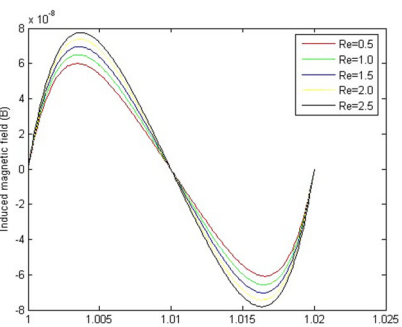


Figure 9. Variation in (B) with Re

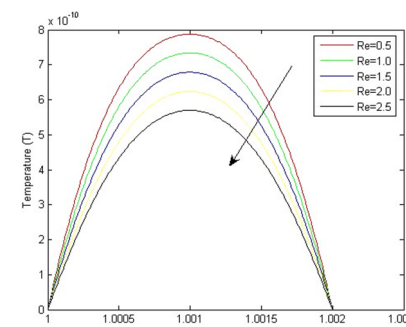


Figure 10. Variation in (T) with Re

Similar effect we have observed in induced magnetic field in **Figure 12**. The temperature distribution of titanium oxide/water nanofluid for those distinct values of Prandtl number (Pr) is depicted in **Figure 13**. But it is observed from **Figure 13**, that the fluid temperature distribution decreases due to increase in value of Prandtl number (Pr). With the large value of (Pr), the momentum diffuses additional rapidly than the heat, indicating that fluids with a large Prandtl number have low thermal conductivity and an exquisite thermal boundary layer. The velocity distribution of titanium oxide/water nanofluid for different values of Eckert number (Ec) is observed in **Figure 14**. We have seen in **Figure 14**, that the fluid velocity distribution decreases due to increase in value of Eckert number (Ec). Again, owing to increase in values of Eckert number (Ec), the plate decants velocity increases. This in turn again decreases the flow rate within the boundary layer and thus diminishes the velocity. Similar pattern is observed in

Figure 15. The temperature distribution of titanium oxide/water nanofluid for different values of Eckert number (Ec) is depicted in **Figure 16**. We have seen in **Figure 16**, that the fluid temperature profile enhanced owing to enhancement in parametric values of Eckert number (Ec). Owing to enhanced in values of (Ec), the fluid occurrence frictional heating in the middle layers, furthermore, there is the thickening of thermal boundary layer and consequently increases the temperature within the boundary layer significantly.

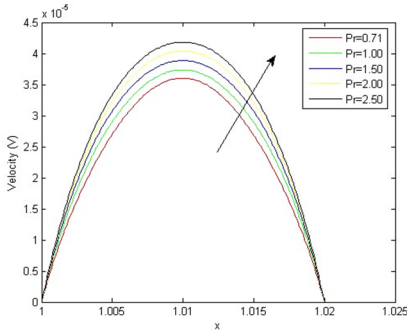


Figure 11. Variation in (V) with Pr

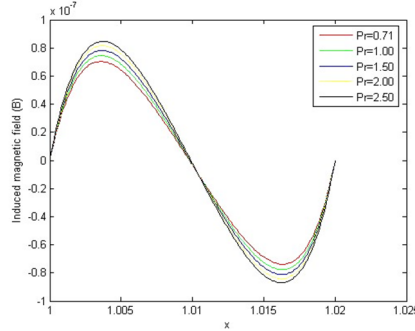


Figure 12. Variation in (B) with Pr

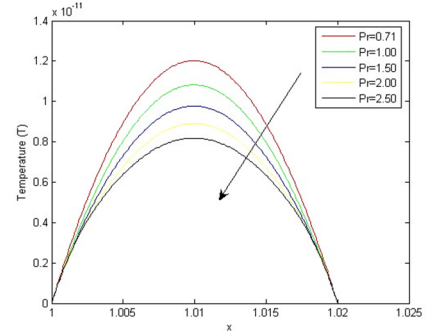


Figure 13. Variation in (T) with Pr

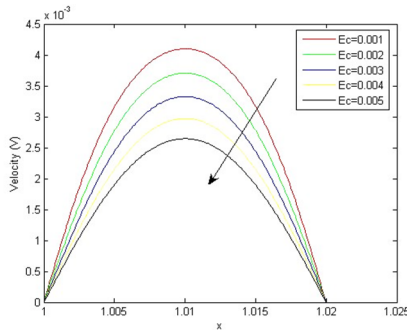


Figure 14. Variation in (V) with Ec

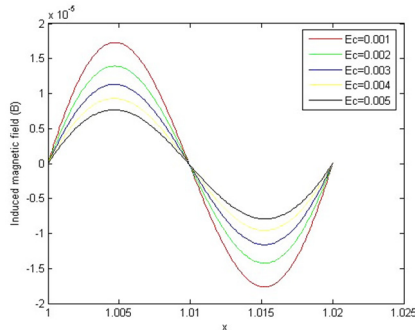


Figure 15. Variation in (B) with Ec

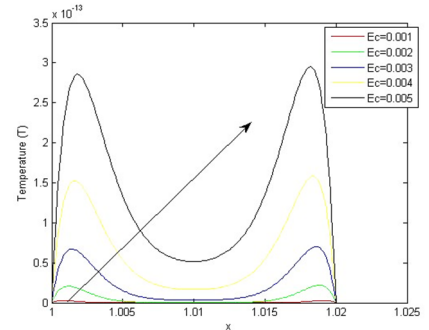


Figure 16. Variation in (T) with Ec

The velocity distribution of titanium oxide/water nanofluid for distinct values of magnetic Reynolds number (R_m) is illustrate in **Figure 17**. We have seen in **Figure 17**, that the fluid velocity distribution increases due to increase in parametric value of magnetic Reynolds number (R_m). The magnetic Reynolds number is the magnetic correspondent of the Reynold number, a fundamental dimensionless classification that take place in magnetohydrodynamics (MHD). It gives an estimate of the respective effects of convective of a magnetic field by the movement of a conducting medium, frequently a fluid, to magnetic diffusion. Similar nature we have observed in **Figure 18**. The temperature distribution of titanium oxide/water nanofluid for different values of magnetic Reynolds number (R_m) is depicted in **Figure 19**. But we have seen in **Figure 19**, that the temperature profile decreases owing to enhancement in parametric values of magnetic Reynolds number (R_m). The enhanced in values of (R_m) enhanced the strength of the decant velocity on the plate and this decant velocity minimizes the growth of thermal boundary layer. Thus, as a consequence diminishes the temperature near to the plate surface.

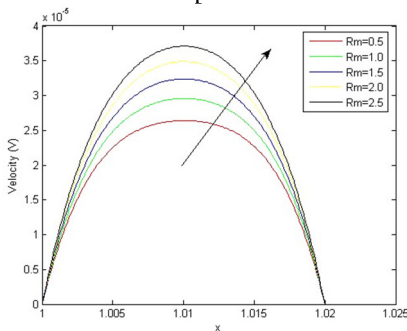


Figure 17. Variation in (V) with Rm

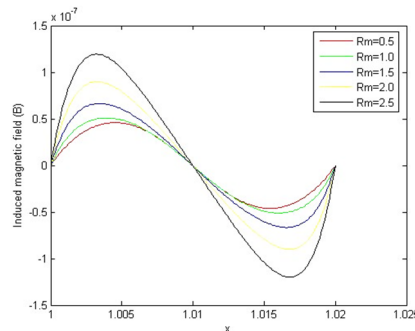


Figure 18. Variation in (B) with Rm

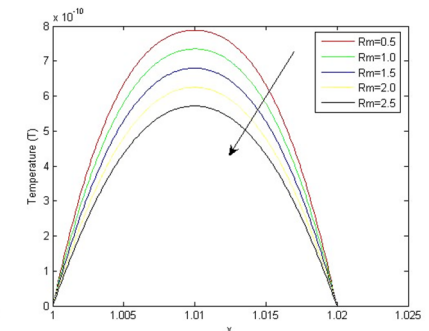


Figure 19. Variation in (T) with Rm

The velocity distribution of titanium oxide/water nanofluid for different values of nanoparticle volume fraction (ϕ) is illustrate graphically in **Figure 20**. We have seen in **Figure 20**, that the fluid velocity distribution decreases due to increase in value of nanoparticle volume fraction (ϕ). Similar pattern is in **Figure 21**, where induced magnetic field variation is shown against volume fraction. The temperature distribution of titanium oxide/water nanofluid for different values of nanoparticle volume fraction (ϕ) is depicted in **Figure 22**. But it is observed from **Figure 22**, that the temperature profile enhanced owing to enhancement in parametric value of nanoparticle volume fraction (ϕ).

We have plotted (Figure 23) values of rate of rise leading velocity for different nanofluids against value of corresponding Reynold number (Re) in the duct under same configuration. We have plotted the graphs for the following nanofluid: titanium oxide (TiO_2), aluminium oxide (Al_2O_3), ferric oxide (Fe_2O_3) and silicon oxide (SiO_2). These plottings provides us a comparative mass transfer advantages of different nano fluids at a certain temperature. From the plottings of (Figure 23), we have seen that with increasing Reynold number (Re) difference of flow rate for different nano fluids is reducing. For low value of Reynold number (Re), ferric oxide (Fe_2O_3) gives high flow rate and silicon oxide (SiO_2) gives low flow rate. For high Reynold number Re all the nanofluid consider shows no significance different in volumetric flow rate.

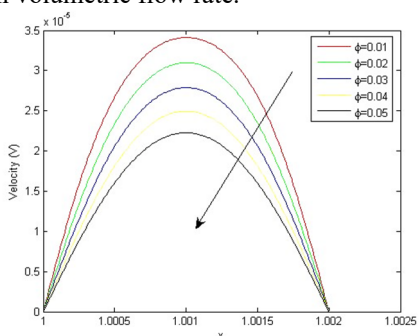


Figure 20. Variation in (V) with ϕ

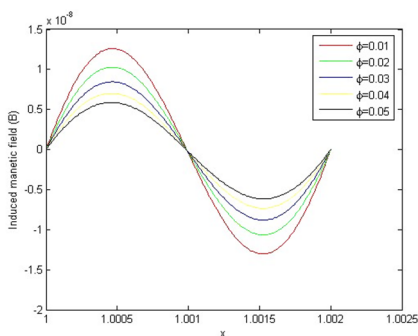


Figure 21. Variation in (B) with ϕ

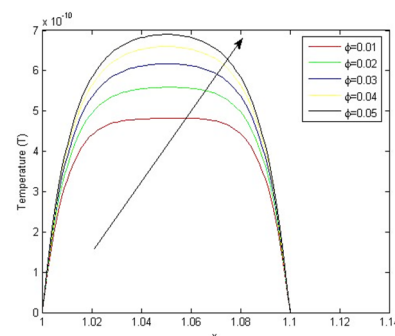


Figure 22. Variation (T) with ϕ

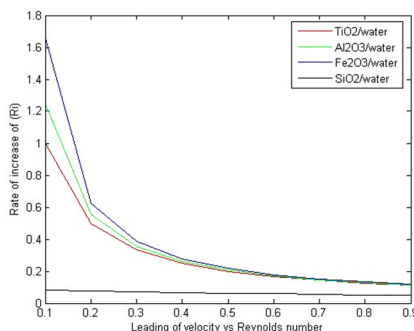


Figure 23. Rate of increase of Reynolds number for (TiO_2), (Al_2O_3), (Fe_2O_3) and (SiO_2) nanoparticles

We have plotted in Figure 24 mesh (x, y, V) for ($Ha = 0$), in Figure 25 contour (x, y, V) for ($Ha = 10$), in Figure 26 mesh (x, y, B) for ($Ha = 0$), in Figure 27 contour (x, y, B) for ($Ha = 10$), in Figure 28 mesh (x, y, T) for ($Ha = 0$), in Figure 29 contour (x, y, T) for ($Ha = 10$) i.e. in the absence of magnetic field for velocity and nanoparticle volume fraction ($\phi = 0.02$). i.e when ($Ha = 0$), the velocity of the TiO_2 – water nanofluid decreases with increase in nanoparticles volume fraction ϕ . In this case 100×100 grid has been used at $x(1) = -1$ and $y(1) = -1$. And another study, in Figure 30 mesh (x, y, V) for ($Ha = 10$), in Figure 31 contour (x, y, V) for ($Ha = 10$), in Figure 32 mesh (x, y, B) for ($Ha = 10$), in Figure 33 contour (x, y, B) for ($Ha = 10$), in Figure 34 mesh (x, y, T) for ($Ha = 10$), in Figure 35 contour (x, y, T) for ($Ha = 10$) i.e. in the presence of large magnetic field and nanoparticle volume fraction ($\phi = 0.02$) for titanium oxide nanoparticle. i.e when ($Ha = 10$) the reverse effect of the nanoparticle volume fraction ϕ . Similarly, we can show for other nanoparticles.

3D graph for TiO_2 – water nanofluid

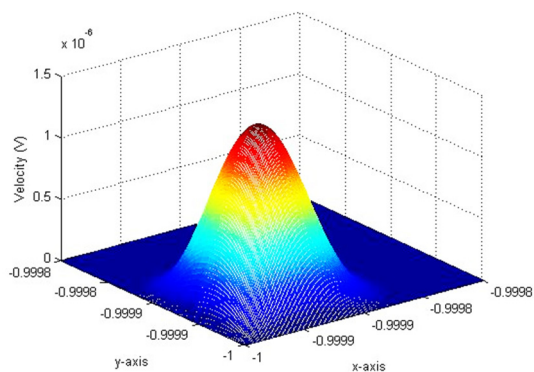


Figure 24. Velocity mesh in (x, y, V) with $Ha = 0, \phi = 0.02$,

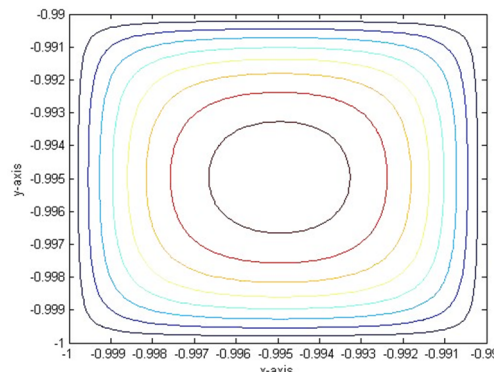


Figure 25. Velocity contour in (x, y, V) $Ha = 10, \phi = 0.02$

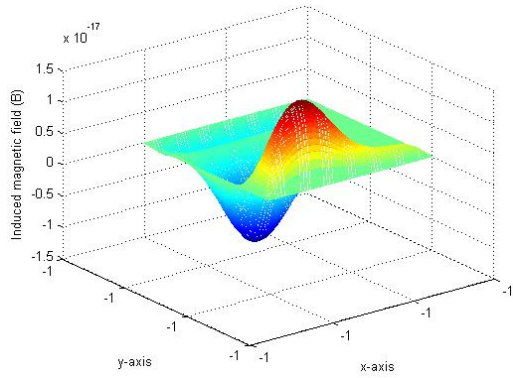


Figure 26. Velocity mesh in (x, y, B) with $Ha = 0, \phi = 0.02$

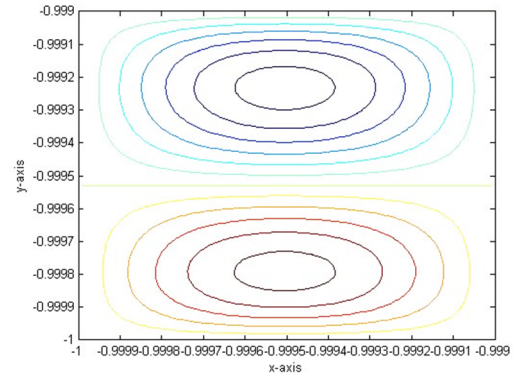


Figure 27. Velocity contour in (x, y, B) $Ha = 10, \phi = 0.02$

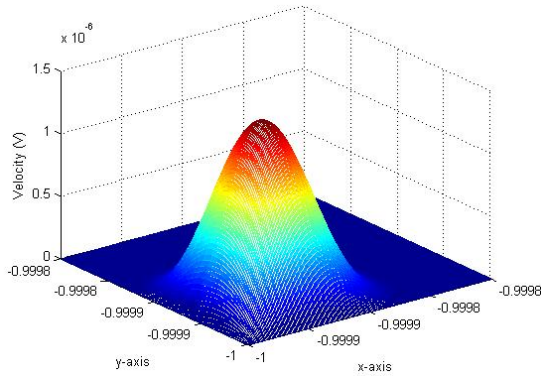


Figure 28. Velocity mesh in (x, y, T) with $Ha = 0, \phi = 0.02$

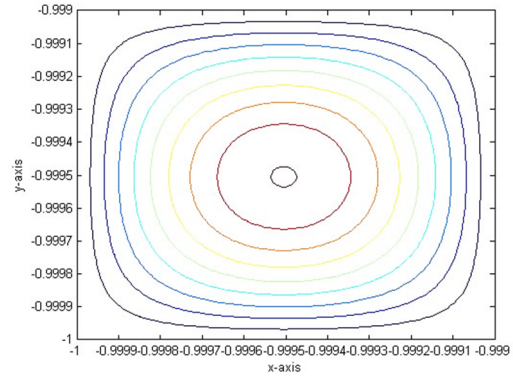


Figure 29. Velocity contour in (x, y, T) $Ha = 10, \phi = 0.02$

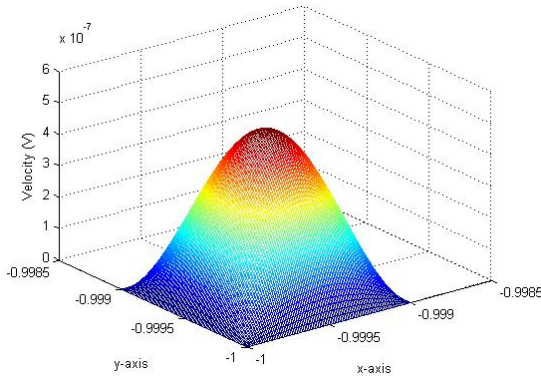


Figure 30. Velocity mesh in (x, y, V) with $Ha = 10, \phi = 0.02$

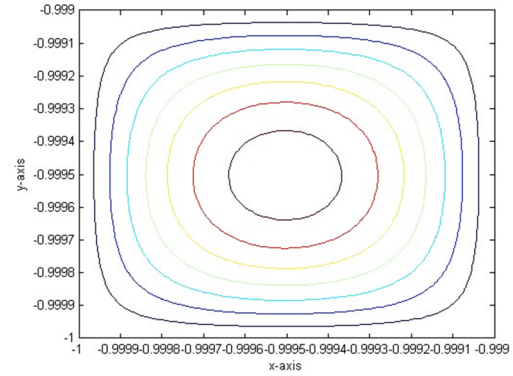


Figure 31. Velocity contour in (x, y, V) $Ha = 10, \phi = 0.02$

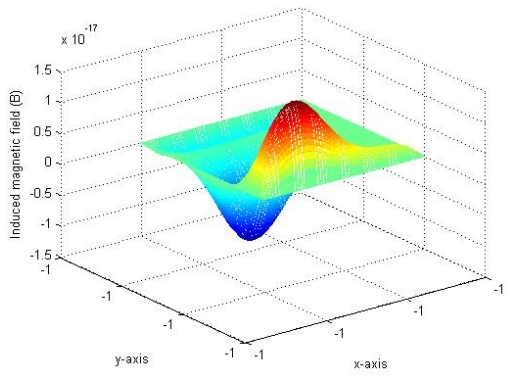


Figure 32. Velocity mesh in (x, y, B) with $Ha = 10, \phi = 0.02$

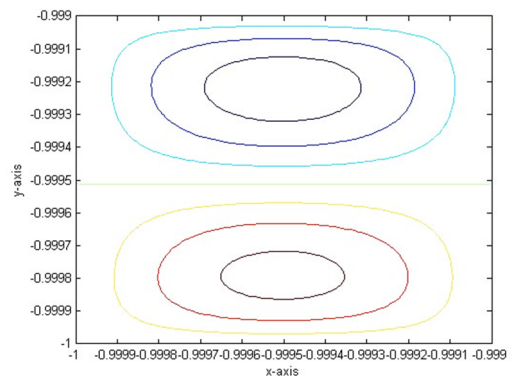


Figure 33. Velocity contour in (x, y, B) $Ha = 10, \phi = 0.02$

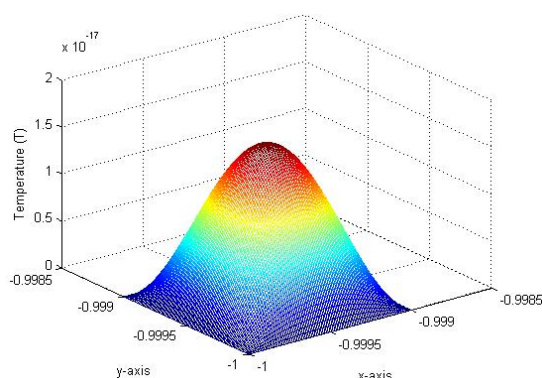


Figure 34. Velocity mesh in (x, y, T) with $Ha = 10, \phi = 0.02$

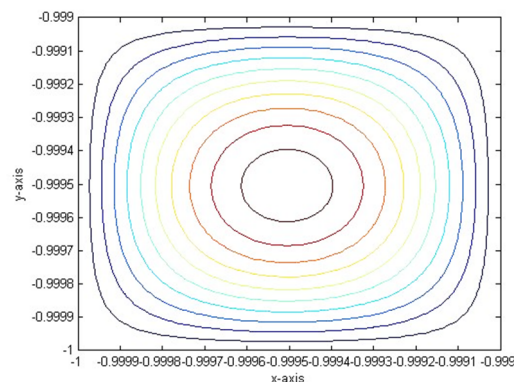


Figure 35. Velocity contour in (x, y, T) with $Ha = 10, \phi = 0.02$

6. CONCLUSIONS

In this paper, a comparative study on MHD forced convective flow for heat transfer efficiency of different nanofluids with water (H_2O) as base fluid has been carried out. Here, in this study flow through vertical rectangular has been considered in presence of strong magnetic field. An explicit finite difference method has been adopted with fine grid in the control volume for solving the governing equation of this MHD nanofluid flow. Computational process is carried out using MATLAB code. In this paper we have plotted the flow fields velocity, induced magnetic field and temperature for various values of MHD flow parameters graphically. The remarkable results of the examination are as follows:

1. From the plottings of (Fig. 23), we have seen that with increasing Reynold number (Re) difference of flow rate for different nano fluids is reducing. For low value of Reynold number (Re) ferric oxide (Fe_2O_3) gives high flow rate and silicon oxide (SiO_2) gives low flow rate. For high Reynold number (Re) all the nanofluid consider shows no significance different in volumetric flow rate.
2. The fluid velocity decreases due to increase in Hartmann number (Ha), Eckert number (Ec) and nanoparticle volume fraction (ϕ).
3. The fluid velocity increases due to increase in Reynold number (Re), thermal Grashof number (G_r), Prandtl number (P_r) and magnetic Reynolds number (R_m).
4. The induced magnetic field decreases due to increase in Hartmann number (Ha), nanoparticle volume fraction (ϕ), and Eckert number (Ec).
5. The induced magnetic field increases due to increase in Reynold number (Re), thermal Grashof number (G_r), Prandtl number (P_r) and magnetic Reynolds number (R_m).
6. The fluid temperature of decreases due to increase in Reynold number (Re), thermal Grashof number (G_r), Prandtl number (P_r) and magnetic Reynolds number (R_m).
7. An increase in values of Hartmann number (Ha), Eckert number (Ec), and nanoparticle volume fraction (ϕ) increases the fluid temperature.

Nomenclature

\vec{V} velocity vector	p fluid pressure, [Pa]	σ electrical conductivity, [$S m^{-1}$]
\vec{J} current density	θ oblique angle	ρC_p effective heat capacity of the nanoparticle, [$J m^{-3} K^{-1}$]
B_0 magnetic field	T temperature of the fluid, [K]	ϕ volume fraction, [-]
C_p specific heat at constant pressure, [$J kg^{-1} K^{-1}$]	ρ_{nf} nanofluid density	λ magnetic diffusivity
\vec{E} electric field	σ_{nf} nanofluid electrical conductivity	μ dynamic viscosity
Ha Hartmann number	μ_{nf} nanofluid dynamic viscosity	Subscripts
G_r thermal Grashof number	k_{nf} nanofluid thermal conductivity	nf nanofluids
Re Reynold number	$(\mu_e)_{nf}$ nanofluid magnetic permeability	f base fluid
P_r Prandtl number	ν_{nf} nanofluid kinematic viscosity	s solid particles of nanofluid
Ec Eckert number		
R_m magnetic Reynolds number		
k thermal conductivity of nanofluid, [$W m^{-1} K^{-1}$]		

Greek Letters

ρ density, [$kg m^{-3}$]
 ν kinematic viscosity, [$m^2 s^{-1}$]

ORCID

REFERENCES

- [1] S.U.S. Choi, "Enhanced thermal conductivity of nanofluids with nano particles, development and applications of Newtonian flows," *FED*, **231**/MD, 99-105 (1995).
- [2] S. Lee, S.U.S. Choi, S. Li, and J.A. Eastman, "Measuring Thermal Conductivity of Fluids Containing Oxide Nanoparticles," *Journal of Heat Transfer*, **121**(2), 280-289 (1999). <https://doi.org/10.1115/1.2825978>
- [3] Y. Xuan, and Q. Li, "Heat transfer enhancement of nano-fluids," *Int. J. Heat Fluid Flow*, **21**, 58-64 (2000). [https://doi.org/10.1016/S0142-727X\(99\)00067-3](https://doi.org/10.1016/S0142-727X(99)00067-3)
- [4] S.K. Das, S.U.S. Choi, Yu. and W. Pradet, *Nanofluids: Science and Technology*, (Wiley, New Jersey, 2007).
- [5] S. Kakac, and A. Parmuanjaroenkij, "Review of Convective Heat Transfer Enhancement with Nanofluids," *International Journal of Heat Mass Transfer*, **52**, 3187-3196. <http://dx.doi.org/10.1016/j.ijheatmasstransfer.2009.02.006>, (2009)
- [6] R. Ellahi, M. Hassan, and A. Zeeshan, "Aggregation Effects on Water Base Al₂O₃- Nanofluid over Permeable Wedge in Mixed Convection", *Asia-Pacific Journal of Chemical Engineering*, **11**, 179-186 (2015). <https://dx.doi.org/10.1002/apj.1954>
- [7] M.A.A. Hamad, "Analytical Solution of Natural Convection Flow of a Nanofluid over a Linearly Stretching Sheet in the Presence of Magnetic Field," *International Communications in Heat and Mass Transfer*, **38**, 487-492 (2011). <http://dx.doi.org/10.1016/j.icheatmasstransfer.2010.12.042>
- [8] R. Kodi, C. Ganteda, A. Dasore, M.L. Kumar, G. Laxmaiah, M.A. Hasan, S. Islam, and A. Razak, "Influence of MHD mixed convection flow for Maxwell nanofluid through a vertical cone with porous material in the existence of variable heat conductivity and diffusion," *Case Stud. Therm. Eng.* **44**, 102875 (2023). <https://doi.org/10.1016/j.csite.2023.102875>
- [9] E. Ragulkumar, G. Palani, P. Sambath, and A.J. Chamkha, "Dissipative MHD free convective nanofluid flow past a vertical cone under radiative chemical reaction with mass flux," *Sci. Rep.* **13** (1), 2878 (2023). <https://doi.org/10.1038/s41598-023-28702-0>
- [10] T. Hayat, M.B. Ashraf, S.A. Shehzad, and A. Alsaedi, "Mixed Convection Flow of Casson Nanofluid over a Stretching Sheet with Convectively Heated Chemical Reaction and Heat Source/Sink," *J. Appl Fluid Mechanics*, **8**, 803-813 (2015). <http://doi.org/10.18869/acadpub.jafm.73.238.22995>
- [11] M. Ferdows, M.D. Shamshuddin, S.O. Salawu, and K. Zaimi, *SN Appl. Sci.* **3**, 264 (2021). <https://doi.org/10.1007/s42452-021-04224-0>
- [12] S. Rao, and P.A. Deka, "Numerical investigation on Transport Phenomena in a Nanofluid Under the Transverse Magnetic Field Over a Stretching Plate Associated with Solar Radiation," in: *Nonlinear Dynamics and Applications*, edited by S. Banerjee, and A. Saha, (Springer Proceedings in Complexity, Springer, Cham, 2022), pp. 473-492. https://doi.org/10.1007/978-3-030-99792-2_39
- [13] S. Rao, and P.A. Deka, "Numerical solution using EFDm for unsteady MHD radiative Casson nanofluid flow over a porous stretching sheet with stability analysis," *Heat Transfer*, **51**(8), 8020-8042 (2022). <https://doi.org/10.1002/htj.22679>
- [14] B.R. Das, P.N. Deka, and S. Rao, "Numerical analysis on MHD mixed convection flow of aluminium-oxide/water nanofluids in a vertical square duct," *East European Journal of Physics*, **2**, 51-62 (2023). <https://doi.org/10.26565/2312-4334-2023-2-02>
- [15] V. Rajesh, A.J. Chamkha, and M.P. Mallesh, "Transient MHD Free Convection Flow and Heat Transfer of Nanofluid past an Impulsively Started Semi-Infinite Vertical Plate," *Journal of Applied Fluid Mechanics* **9**, 2457-2467 (2015). <https://doi.org/10.18869/acadpub.jafm.68.236.23443>
- [16] M. Jawad, M.K. Hameed, K.S. Nisar, A.H. Majeed, "Darcy-Forchheimer flow of Maxwell nanofluid flow over a porous stretching sheet with Arrhenius activation energy and nield boundary conditions," *Case Studies in Thermal Engineering*, **44**, 102830 (2023). <https://doi.org/10.1016/j.csite.2023.102830>
- [17] A. Paul, and T.K. Nath, "Darcy -Forchheimer MHD radiative flow through a porous space incorporating viscous dissipation, heat source, and chemical reaction effect across an exponentially stretched surface," *Heat Transfer*, **52** (1), 807-825 (2023). <https://doi.org/10.1002/htj.22717>
- [18] C.A. Nandhini, S. Jothimani, and A.J. Chamkha, "Effect of chemical reaction and radiation absorption on MHD Casson fluid over an exponentially stretching sheet with slip conditions: ethanol as solvent," *The European Physical Journal Plus*, **138**(1), 1-17 (2023). <https://doi.org/10.1140/epjp/s13360-023-03660-8>
- [19] H. Alrihili, M. Alrehili, and A.M. Megahed, "Radiative MHD Nanofluid Flow Due to a Linearly Stretching Sheet with Convective Heating and Viscous Dissipation," *Mathematics*, **10**(24), 4743 (2022). <https://doi.org/10.3390/math10244743>
- [20] M. Jawad, "A Computational Study on MHD Stagnation Point Flow of Micropolar Fluids with Buoyancy and Thermal Radiation due to a Vertical Stretching Surface," *Journal of Nanofluids*, **12**(3), 759-766 (2023). <https://doi.org/10.1166/jon.2023.1958>
- [21] S. Shoeibi, H. Kargarsharifabad, N. Rahbar, G. Ahmadi, M.R. and Safaei, "Performance evaluation of a solar still using hybrid nanofluid glass cooling- CFD simulation and environmental analysis," *Sustainable Energy Technologies and Assessments*, **49**, 101728 (2022). <https://doi.org/10.1016/j.seta.2021.101728>
- [22] O.A. Beg, and J.C. Umavathi, "Computation of thermo-solutal convection with Soret-Dufour cross diffusion in a vertical duct containing carbon/metallic nanofluids," in: *Proceedings of the Institution of Mechanical Engineers, Part C: Journal of Mechanical Engineering Science*, **236**(13), (2022). <http://dx.doi.org/10.1177/09544062211072693>
- [23] M.M. Bhatti, M.B. Arain, A. Zeeshan, R. Ellahi, and M.H. Doranehgard, "Swimming of Gyrotactic microorganism in MHD Williamson nanofluid flow between rotating circular plates embedded in porous medium: Application of thermal energy storage," *J. of Energy Storage*, **45**, 103511 (2021). <https://doi.org/10.1016/j.est.2021.103511>
- [24] Z. Hussain, A.U. Rehman, R. Zeeshan, F. Sultan, T.A. Hamid, M. Ali, and M. Shahzad, "MHD instability of Hartmann flow of nanoparticles Fe₂O₃ in water," *Appl. Nanosci.* **10**, 5149-5165 (2020). <https://doi.org/10.1007/s13204-020-01308-y>
- [25] J.C. Umavathi, and O.A. Beg, "Double diffusive convection in a dissipative electrically conducting nanofluid under orthogonal electrical and magnetic fields: a numerical study," *Nanoscience and Technology: An International Journal*, **12**(2), 59-90 (2021). <https://doi.org/10.1615/NanoSciTechnolIntJ.2021036786>
- [26] M.M. Bhatti, and S.I. Abdelsalam, "Bio-inspired peristaltic propulsion of hybrid nanofluid flow with Tantalum (Ta) and Gold (Au) nanoparticles under magnetic effects," *Waves in Random and Complex Media*, 1745-5030 (2021). <https://doi.org/10.1080/17455030.2021.1998728>

ПОРІВНЯЛЬНЕ ДОСЛІДЖЕННЯ МГД ПРИМУШЕНОГО КОНВЕКТИВНОГО ПОТОКУ РІЗНИХ НАНОРІДИН З ВОДОЮ (H₂O) ЯК ОСНОВНОЮ РІДИНОЮ У ВЕРТИКАЛЬНОМУ ПРЯМОКУТНОМУ КАНАЛІ**Бішну Рам Дас, П.Н. Дека***Факультет математики, Університет Дібругарх, Дібругарх-786004, Ассам, Індія*

У цій статті було проведено порівняльне дослідження МГД вимушеної конвективної течії для ефективності теплопередачі різних нанофлюїдів з водою (H₂O) як базовою рідиною. У цьому дослідженні потік через вертикальний прямокутний канал розглядався в присутності сильного магнітного поля. У цьому ламінарному потоці ми розглядаємо стінки каналу як електрично непровідні, де поперечне магнітне поле діє нормально на стінки каналу. Джоулева теплота та ефекти розсіювання в'язкої рідини враховуються в енергетичному рівнянні, і, крім того, стінки каналу зберігаються при постійній температурі. Було прийнято явний кінцево-різницеви метод із дрібною сіткою в контрольному об'ємі для розв'язання керівних рівнянь цього МГД-потіку нанорідини. Обчислювальні процеси здійснюються за допомогою коду MATLAB. У цій роботі ми графічно побудували графіки швидкості полів потоку, індукованого магнітного поля та температури для різних значень МГД параметрів потоку шляхом зміни теплового числа Грасгофа (G_r), числа Гартмана (H_a), числа Рейнольдса (Re), числа Екерта (Ec), числа Прандтля (Pr), магнітне число Рейнольдса (R_m) і об'ємну частку наночастинок (ϕ) відповідно.

Ключові слова: *вимушена конвективна МГД течія; нанофлюїди; стійкий; явний метод кінцевих різниць (EFDM); вертикальний прямокутний канал*